

Design of Rectangular Patch Antenna on the Hilbert Fractal-shaped High Impedance Surface

Akash Kumar Gupta^{1,2*}, P Satish Rama Chowdary² & M Vamshi Krishna³

¹Department of ECE, Centurion University of Technology and Management, Odisha, 761 211 India

²Department of ECE, Raghu Institute of Technology, Visakhapatnam, 531 162, Andhra Pradesh, India

³Department of ECE, Dhanekula Institute of Engineering and Technology, Vijayawada, 521 139, Andhra Pradesh, India

Received 17 August 2022; revised 21 September 2022; accepted 07 October 2022

The high Impedance Technique has emerged as a modern approach for high-gain microstrip antennas. A high impedance surface minimizes surface waves and provides increased gain. Instead of, a typical mushroom to design High Impedance Surface (HIS), fractal geometry can be used. Hilbert curve-based Fractal geometry minimizes physical length and keeps electrical length the same. In this work, three iterations of Hilbert curve-shaped HIS geometry are studied with emphasis on HIS application. Fractal facilitates multi-frequency operation from GSM 1800 MHz to 6 GHz Wireless applications. The antennas have a peak gain of 5.3 dBi. The simulation is conducted in HFSS, and the analysis is performed using reports like reflection coefficients, radiation patterns, and gain plots

Keywords: Fractal geometries, High impedance surfaces, Hilbert curves

Introduction

The general structure of the patch antenna includes a dielectric substrate between two Conducting plates. The metallic ground plane is a reflector reflecting the antenna's radiation towards the front. However, the metallic ground has a disadvantage as it allows surface waves that travel within the plane to end or corner to get radiation into free space. These Surface waves result in multipath propagation and reduction of gain. Destructive or degrading interference is another drawback that is caused due to ground reflected waves. These surface waves subsequently result in distortions and gain contractions.

To overcome the above-listed problems, an Electromagnetic Band Gap (EBG) is often considered a solution.¹ The surface wave propagation is shown in Fig. 1(a), and Fig. 1(b) shows the suppression of surface waves using EBG structures. The proposed geometry consists of a periodic pattern of small metal patches connecting the ground plane through the vias; such arrangement is known as high impedance surfaces. The periodic pattern is the metallic conductor and can be several other materials. Because of its significant and unique electromagnetic

properties, HIS has been widely adopted to design next-generation antennas and filters.

A high impedance surface antenna is widely used for bandwidth enhancement. Falkner *et al.*² used mushroom-shaped HIS for bandwidth enhancement, and curl loading with HIS is used in Wu *et al.*³ to enhance the antenna's bandwidth. The structures are

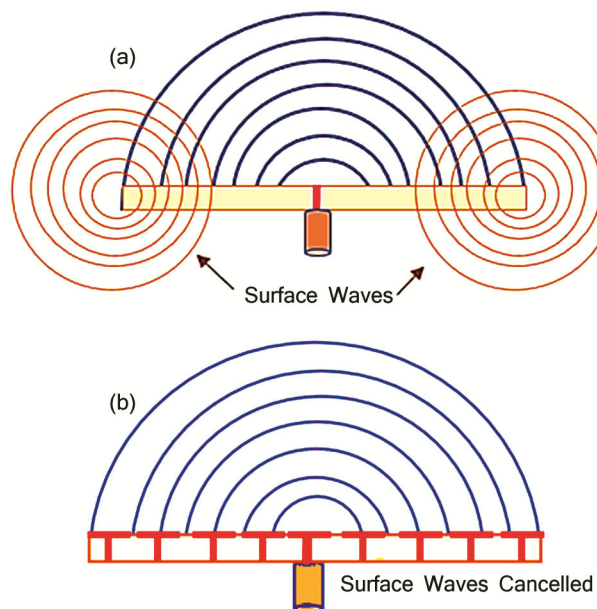


Fig. 1 — (a) Surface waves on Ground plane (b) HIS

*Author for Correspondence
E-mail: ak Gupta452@gmail.com

capable of managing the resonant and non-resonant bands effectively. Maryam *et al.*⁴ reports the use of symmetrical HIS in form of mushrooms for TM_{10} and quasi- TM_{20} mode resonant frequencies. The HIS is coherently capable of exhibiting the forbidden band characteristics. Bait *et al.*⁵ used a double-band dual-sided high-impedance surface (DB-DS-HIS) for band rejection applications. The primary antenna is designed for band rejection response at two bands (X band and Ku band). As the structures allow radiating planes much closer to the ground, it significantly contributes to the low-profile antenna.^{3,6-10} Low-profile antenna designing is also possible using the HIS technique. HIS also finds various applications for multiband antennas^{5,11} and presents a frequency-reconfigurable antenna for triple band operation where a quasi-Sierpinski antenna is fabricated on dual-band HIS with square slots. Similarly, it also isolates the radiating system as the radiating plane need not be subjected to direct ground plane shorting. HISs are artificial magnetic conductors (AMCs) frequently employed in designing low-profile antennas and miniaturized electromagnetic absorbers. Frequency Selective Surfaces are often backed by HIS plane.¹² HIS-backed antennas are also helpful in designing Frequency selective surface antennas.^{12,13} HIS-backed antennas are also having ease of Design for Tuneable antennas¹³ and reconfigurable antennas¹¹, and wearable antennas.^{6,10} The low profile of HIS makes it suitable for RCS and telemetry applications.^{5,14} It is also useful to design multilayer designs.¹⁵ The HIS structures have different shapes like square mushroom^{16,17}, slotted square^{13,18,19}, rectangular^{3,6,7,20}, circular¹⁰, dog-bone²⁰, chess board⁵, Hexagonal fractals²¹ and fractals like Sierpinski.¹¹ The fractal antennas have the advantage of miniaturization in that a large electrical length is obtained over a very small physical area and these structures are not explored much. In this work Fractal antenna with Hilbert curve, geometry is investigated for HIS applications.

HIS Design Methodology

HIS Structure

The HIS structures consist of a 2-D array of Limited rows and limited columns of microstrip antennas, and this arrangement helps suppress surface waves. These microstrip antennas are connected through the ground plane with metallic points (Vias) and configured with an electromagnetic filter. The

Metallic patch with via and the gap between them equivalently act as inductor and capacitor as shown in Fig. 2(a) and Fig. 2(b). The entire periodic Array acts as parallel connections of these inductors and capacitors concerning the ground plane. The sheet impedance of the surface is equivalent to the impedance of resonance of a parallel combination of the sheet inductance(L) and the sheet capacitance(C).

$$Z = \frac{j\omega L}{1-\omega^2 LC} \quad \dots (1)$$

where, z = sheet impedance, C = sheet capacitance L= sheet inductance.

At low frequencies, the HIS plane has an inductive response; at high frequencies, it has a capacitive response. The impedance rises to a point where it is infinite. The resonance frequency is given by,

$$\omega_0 = \frac{1}{\sqrt{LC}} \quad \dots (2)$$

$$\frac{\Delta\omega}{\omega_0} = \frac{\sqrt{L/C}}{\sqrt{\mu_0\epsilon_0}} \quad \dots (3)$$

where, $\Delta\omega$ is bandwidth, and ω_0 is resonance frequency.

$$L = \mu_r\mu_0 t \quad \dots (4)$$

$$C = \frac{W(\epsilon_0+\epsilon_1)}{\pi} \cosh^{-1} \left(\frac{l}{s} \right) \quad \dots (5)$$

where, ' μ_0 ' denotes permeability in free space, ' μ_r ' denotes the relative permeability of the substrate material, 't' denotes the thickness of the dielectric substrate, ' ϵ_1 ' denotes the substrate dielectric constant, 'W' denotes the length of a unit cell, 'l' denotes the distance between neighboring vias, and 's' denotes the spacing between patches. A mushroom-type HIS ground plane as shown in Fig. 3 is designed by Vinoy *et al.*²² using the FEM model to suppress the surface waves using the EBG

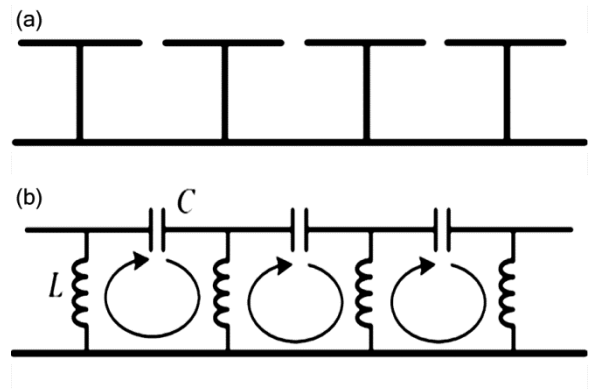


Fig. 2 — (a) an Arrangement of HIS Cells over Mettalic Ground plane (b) Equivalent Circuit

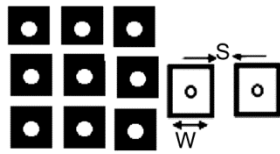


Fig. 3 — HIS Array top view and Crosectional view

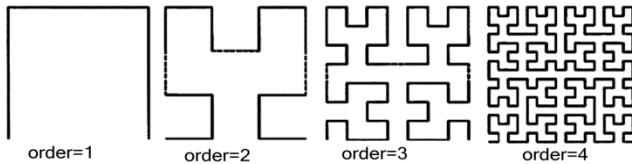


Fig. 4 — Hilbert curve Iterations

technique. The HIS technique and its formulation are validated using the transmission line model, surface impedance model, and finite element method.

Hilbert Curves

Hilbert curves are the most famous space-filling curves. The Hilbert curves were initially proposed by mathematician Hilbert in 1891. Being a space-filling curve, it is an attractive solution for fractal antennas. i.e., a large metallic wire can be made fit into a small area. Thus, it provides space optimization. As the order of iterations increases, the occupancy of the filled-in area increases and accommodates more length of wire.

Hence, a longer wavelength antenna can occupy the minimal physical area. Hilbert curve-based fractal antennas can be used to design miniaturized antennas.²²

The first four iterations of the Hilbert Curve are shown in Fig. 4. It shows that the order of iterations increased, the length of the wire increased, and occupied the same area but with more density. The Design and validation of Hilbert curve-based fractal antennas are performed and validated in Long *et al.*²³

Proposed Fractal-based HIS Design

This work presents a fractal-shaped HIS cell-based antenna design with the simulation performed on HFSS-Ansys Electromagnetic Suite 2019 R3. In this paper, three iterations of Hilbert curve-based HIS antennas are presented. The simulation results are analyzed regarding the radiation pattern, reflection coefficient plot, and 3-D polar plots. The HIS-based ground plane consists of a copper ground plane followed by a dielectric surface and Hilbert fractal-based metallic patches. These fractal patches are connected to the ground plane using vias.

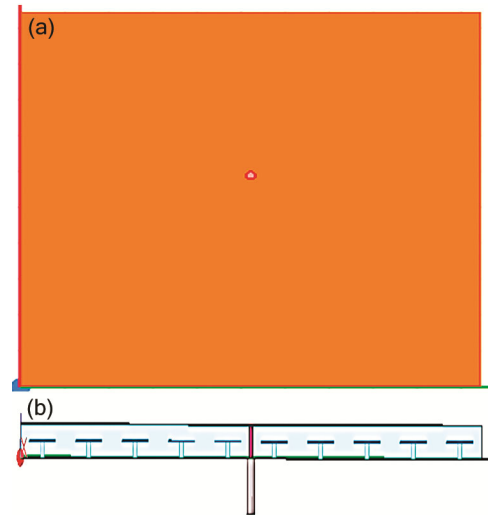


Fig. 5 — Different view of Hil 1-1: (a) Bottom View (b) Cross-sectional view

Hilbert Curve-based HIS Cell

For the dual layer, HIS cell construction is made by evaluating capacitances formed by structural fringing fields between the mushroom patch and the ground plane. Calculations are made with the substrate having dielectric constants 2–10 with a substrate thickness of a few millimeters which results in the capacitance of a few picofarads and inductances of a few nano henrys. The structure has resonant frequencies under 10 GHz. For a dielectric constant of 4–5 with substrate height of 1–2 mm excellent bandgap exists within TE, TM modes for the frequency range of 2.0–2.5 GHz, widely suitable for wireless communications.

The Hilbert curve-based HIS antenna is designed over an FR4 glass epoxy substrate material having a permittivity of 4.4 and a loss tangent of 0.02. The thickness of the substrate height is 1.5 mm. The three iterations of Hilbert curves are designed with a unit square patch length of 10mm, an array of 10×10 , and the gap between unit design is chosen as 0.5 mm. Similarly, another three iterations of Hilbert curves have been designed with a side length of 20 mm, an array size of 5×5 , and a gap of 1 mm. In further sections, Hilbert curves with unit cell obtained for 10×10 mm square patch is referred to as Hil 1 and similarly, Hil 2 refers to unit cell obtained for 20×20 mm square patch.

The cross-section view of the HIS structure is shown in Fig. 5(a) and the metallic ground plane is shown in Fig. 5(b). The Hilbert curve's first iteration with 10×10 Array and 5×5 is shown in Fig. 6(a) &

Fig. 6(b), respectively. The Hilbert curve for the second iteration with 10×10 Array and 5×5 is shown in Fig. 7(a) & Fig. 7(b), respectively. The Hilbert curve for the third iteration with 10×10 Array and 5×5 is shown in Fig. 8(a) & (b), respectively. From each Hilbert curve patch, protrusions of 1 mm diameter are made to the ground plane. Over the HIS ground plane, a rectangular patch antenna is designed for wireless communication applications. The patch dimensions are obtained from Balanis.²⁴ Another layer of FR4 epoxy with a substrate height of 1.5 mm is used between the HIS ground plane and the top rectangular patch. The design details are summarized in Table 1

Results and Discussion

In this section, results pertaining to the simulated models of HIS with Hilbert Fractal antennas with iterations are discussed in terms of return loss (S_{11}), a 2-D plot of the radiation pattern, and a 3D polar gain plot.

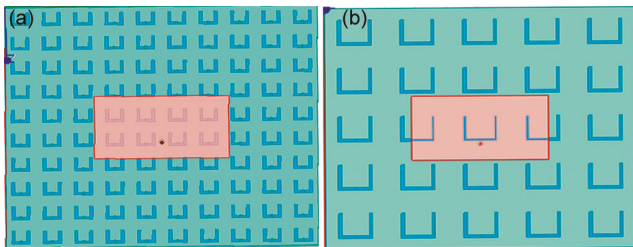


Fig. 6 — Top view (a) Hil 1-1 (b) Hil 2-1

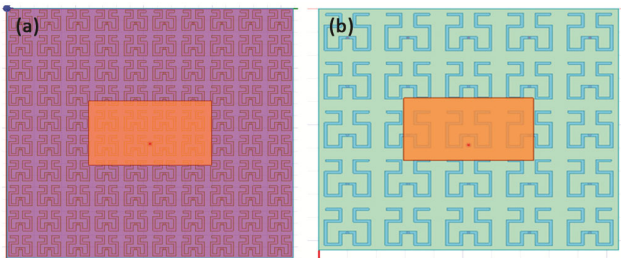


Fig. 7 — Top view (a) Hil 1-2 (b) Hil 2-2

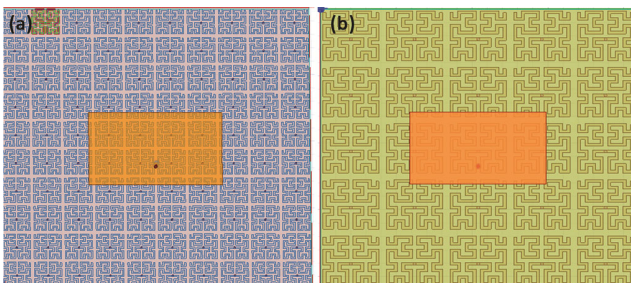


Fig. 8 — Top view (a) Hil 1-3 (b) Hil 2-3

Return Loss

The return loss plot indicates how much power is reflected back and how much power is radiated into space. It is represented as S_{11} for good performance, antenna return loss must be less than -10 dB.

The return loss plot for Hilbert curve iteration 1 based on HIS-backed RMPA is shown in Fig. 9(a). The above response shows that the antenna has a central frequency at 2.1317 GHz, 3.3050 GHz, 4.9 GHz, and 5.2483 GHz with S_{11} of -20.6 , -21.04 , -18.98 , and -16.87 dB, respectively. As per design specifications, the HIS structure has a resonance frequency between 2–2.5 GHz. The simulation results agree with the theoretical calculations. For Hilbert curve fractal with first iterations results in multiple frequency responses.

The Return loss plot for Hil 2_1 is shown in Fig. 9(b). With an increased HIS Hilbert fractal patch length to 20 mm with a gap of 1 mm, the simulated results fall over the desired frequency range of 2.0–2.5 GHz with a decent reflection coefficient (S_{11}) of -11.45 dB. Moreover, has a second response

Table 1 — Design Details for Hilbert Curve shaped HIS

Design Name	Hil 1	Hil 2
Hilbert Curve-HIS unit Cell Dimension (in mm)	10×10	20×20
HIS Array	10×10	5×5
Antenna Dimension(In mm)	104.5×104.5	104.5×104.5
Radiating RMPA dimension ($L_p \times W_p$)(In mm)	27×45	27×45
Substrate 1 thickness (In mm)	1.5	1.5
Substrate 2 thickness (In mm)	1.5	1.5

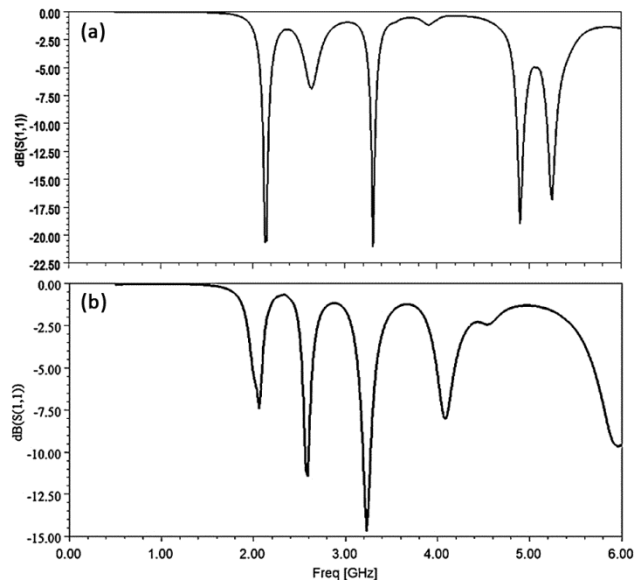


Fig. 9 — The Return loss plots for: (a) Hil 1_1, (b) Hil 2_1

at 3.228 GHz with a reflection coefficient (S_{11}) of -14.688 dB.

The Return loss plot for Hil 1_2 is plotted in Fig. 10(a) i.e., Hilbert curve 2nd iteration based HIS Cell 10×10 array ground plane. With designed specifications, simulation results agreed with the reflection coefficient (S_{11}) of -10.2034 dB at 2.9383 GHz. Due to fractal structures, it will also resonate at other frequencies of 1.78, 3.3233, and 3.9760 GHz.

The Return loss plot for Hil 2_2 is plotted in Fig. 10(b), with an increased HIS Hilbert fractal patch length to 20 mm with a gap of 1 mm. The simulated results fall over the desired frequency range of 2.0–2.5 GHz with a decent reflection coefficient of -19.08 dB, moreover, having multiple responses at 2.656, 3.3820, 4.0420, and 5.9780 GHz.

The Return loss plot for Hil 1_3 is plotted in Fig. 11(a), i.e., Hilbert curve 3rd iteration based HIS Cell 10×10 array ground plane. With designed specifications, simulation results agreed with reflection coefficients of -35.34 dB at 2.3130 GHz. Due to fractal structures, it will also resonate at other frequencies of 2.7611, 3.1685, 3.8815, and 4.4111 GHz.

The Return loss plot for Hil 2_3 is plotted in Fig. 11(b) with an increased HIS Hilbert fractal patch length to 20 mm with a gap of 1 mm. The simulated results fall over the desired frequency range of 2.0–2.5 GHz with a decent reflection coefficient of -19.5352 dB, moreover, having multiple

responses at 0.6833, 2.3517, 2.5167, 3.1033, 4.0383, and 4.1300 GHz.

Radiation Pattern

The radiation pattern of the Hilbert curve-shaped HIS-backed RMPA antenna is shown in Fig. 12. The Hilbert curve's 1st iteration radiation patterns in Fig. 12(a & b) shows a good radiation pattern in which most of the radiation is directed over the upper hemisphere. The pattern for all resonating frequencies is similar and closely concentrated. However, a slight gain reduction is observed for other resonating frequencies apart from 2.0–2.5 GHz. The reduction of gain is due to fractal properties. A similar response was obtained when the HIS cell side length increased to 20 mm and the gap to 1 mm. However, the directivity is slightly improved with null at the back lobe.

Hilbert curve's second iteration Figs 12(c & d) show a good radiation pattern, in which most radiation is directed over the upper hemisphere. The side over radiation is minimized and produces an excellent forward radiation pattern. The pattern for all resonating frequencies is similar and closely concentrated. However, a slight gain reduction is observed for other resonating frequencies apart from 2.0–2.5 GHz. The reduction of gain is due to fractal properties. A similar response is obtained when the patch length increases to 20 mm and the gap to 1 mm. However, the directivity is slightly improved with null at the back lobe.

Hilbert curve's third iteration Fig. 12 (e) and Fig. 12(f) show a good radiation pattern in which

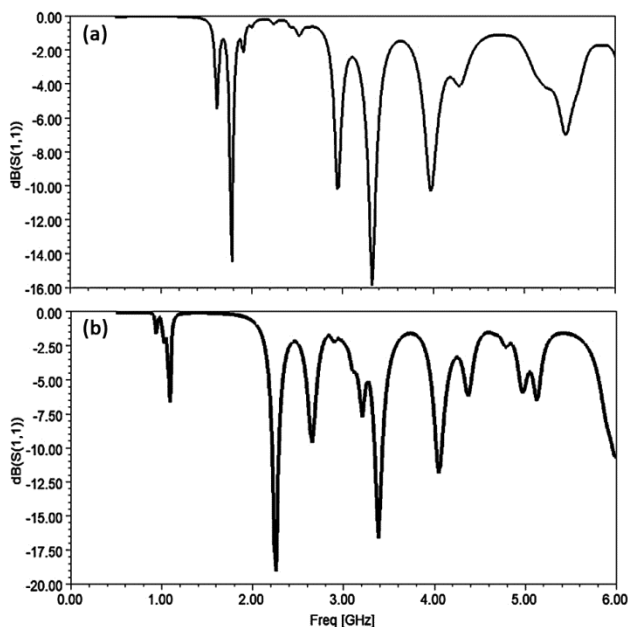


Fig. 10 — The Return loss plots for: (a) Hil 1_2, (b) Hil 2_2

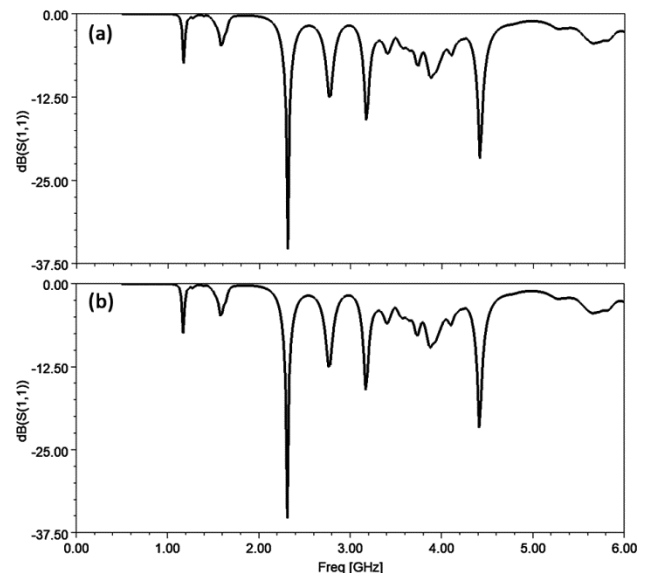


Fig. 11—The Return loss plots for: (a) Hil 1_3, (b) Geometry 2_3

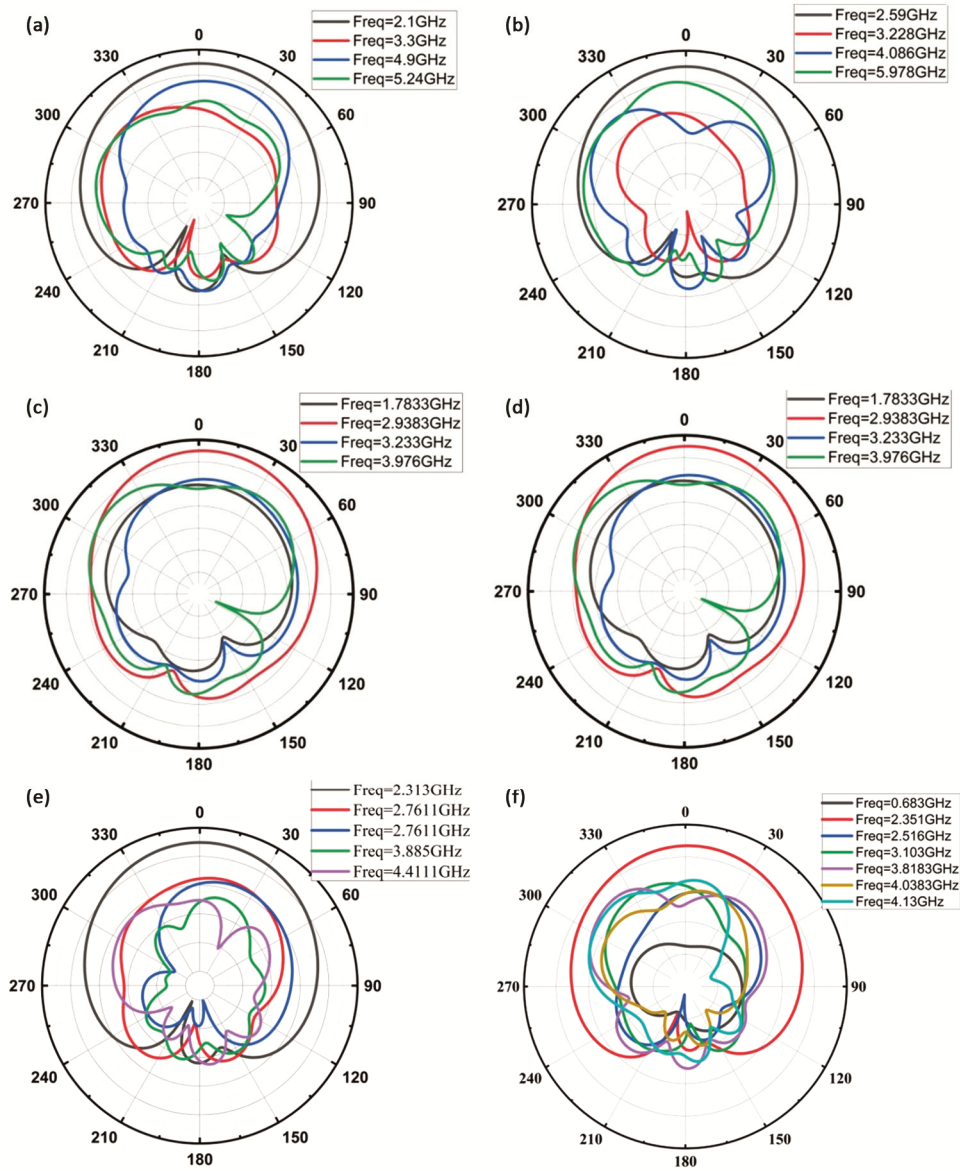


Fig. 12(a-f) — The Radiation Pattern of (a) Hil 1_1, Hil 2_1, (c) Hil 1_2, (d) Hil 2_2, (e) Hil 1_3 and (f) Hil 2_3

most radiation is directed over the upper hemisphere. The pattern for all resonating frequencies is similar and widely concentrated to the 2.0–2.5 GHz pattern. However, significant gain reduction is observed for other resonating frequencies apart from 2.0–2.5 GHz. The reduction of gain is due to fractal properties. A similar response was obtained when the patch length increased to 20 mm and the gap to 1 mm. However, the directivity is slightly improved.

3D- Polar plot for Gain

The 3D polar plots for Hilbert curve fractal-based RMPA are shown in Fig. 13. The gain plot for

hil 1_1 (Fig. 13(a)) has a maximum gain of 4.6 dBi while the gain plot for hil 1_2 (Fig. 13(b)) has a peak gain of 4.8 dBi. The gain plot for hil 1_2 has a peak gain of 5.2 dBi (Fig. 13(c)). The pattern shows that there is no back lobe or side lobes and only radiation in the forward direction. The gain plot for hil 2_2 (Fig. 13(d)) shows a maximum gain of 5.3 dBi. The gain plot for hil 1_3 is shown in Fig. 13(e) and has a maximum gain of 4.9 dBi. The gain plot for hil 2_3 as shown in Fig. 13(f) has a maximum gain of 3.5 dBi. The return loss at central frequencies is summarised in Table 2.

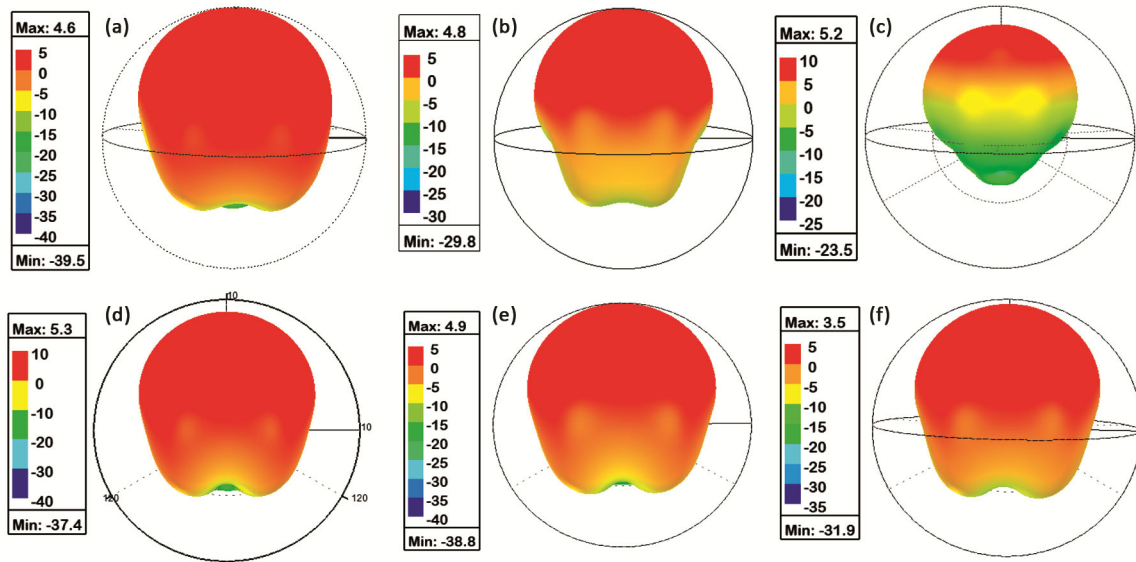


Fig. 13(a-f) — The Polar plot for (a) Hil 1_1, (b) Hil 2_1, (c) Hil 1_2, (d) Hil 2_2, (e) Hil 1_3 and (f) Hil 2_3

Table 2 — Radiating frequencies of HIS-RMPA

HIS structure	Lp = Wp = 10 mm, gap = 0.5 mm		Lp = Wp = 20 mm, gap = 1 mm	
	Centre Frequency (GHz)	Return loss (In dB)	Centre Frequency (In GHz)	Return loss (In dB)
Hilbert curve iteration 1 shaped HIS RMPA	2.1317	-0.6376	2.59	-11.4525
	3.305	-21.0489	3.228	-14.688
	4.9	-18.9807	4.086	-8.0787
	5.2483	-16.8727	5.978	-9.6411
Hilbert curve iteration 2 shaped HIS RMPA	1.7833	-14.4628	2.26	-19.0815
	2.9383	-10.2034	2.656	-9.6284
	3.2333	-15.8645	3.382	-16.612
	3.976	-10.1934	4.042	-11.8831
Hilbert curve iteration 3 shaped HIS RMPA	—	—	5.978	-10.687
	2.313	-35.3418	0.6833	-10.7229
	2.7611	-12.5378	2.3517	-19.5352
	3.1685	-16.0225	2.5167	-15.4408
	3.8815	-9.7129	3.1033	-12.6223
	4.4111	-21.7446	3.8183	-8.3089
—	—	4.0383	-19.0881	
—	—	4.13	-21.9542	

Conclusions

The Hilbert curve fractal-based HIS antenna has been successfully designed and analyzed. High impedance surface act as filters that minimizes surface waves and provides increased gain. The inherent multiband has the advantage of all the features suitable for mobile applications. The Hilbert curve fractal-based antenna has central frequencies from 683 MHz to 5.978 GHz in Wireless applications. The antennas have a peak gain of 5.3 dBi. The performance of the antenna in terms of gain and resonance is studied and analyzed. There is a clear dependency of the resonant frequencies and the multiband characteristics on the iteration number of

the Hilbert Curve. The prototype development and validation would be the best scope of future work.

References

- Gu M, Vorobiev D, Kim W S, Chien H-T, Woo H-M, Hong S C & Park S I, A novel approach using an inductive loading to lower the resonant frequency of a mushroom-shaped high impedance surface, *Prog Electromagn Res M*, **90** (2020) 19–26.
- Falkner B J, Zhou H, Mehta M, Arampatzis T, Mirshekar D S & Nakano H, A circularly polarized low-cost flat panel antenna array with a high impedance surface meta-substrate for satellite on-the-move medical iot applications, *IEEE Trans Antennas Propag* **69(9)** (2021) 6076–6081, DOI: 10.1109/TAP.2021.3070011.
- Wu T, Chen J & Wu P F, Multi-mode high-gain antenna array loaded with high impedance surface, *IEEE Access*, **8**

- (2020) 147070–147076, DOI: 10.1109/ACCESS.2020.3015758.
- 4 Maryam S H, Bemani Md & Saeid N, A novel dual-band double-sided high-impedance surface (DB-DS-HIS) with systematic design methodology, *AEU - Int J Electron Commun*, **115** (2020) 153039, <https://doi.org/10.1016/j.aeue.2019.153039>
 - 5 Bait S, Mohammed M, Isidoro I L & Akram A, Impedance enhancement of textile grounded loop antenna using high-impedance surface (HIS) for healthcare applications, *Sensors* **20(14)** (2020) <https://doi.org/10.3390/s20143809>
 - 6 SoltaniS, Dusenbury J & Kerby-Patel K C, Multiconductor transmission line model for an antenna with high-impedance ground plane, *IEEE Trans Antennas Propag*, **19(12)** (2020) 2097–2101, DOI: 10.1109/LAWP.2020.3023378.
 - 7 Panda P K & Ghosh D, Wideband and high gain tuning fork-shaped monopole antenna using high impedance surface, *AEU - Int J Electron Commun*, **111** (2019) 152920, <https://doi.org/10.1016/j.aeue.2019.152920>
 - 8 Panda P & Ghosh D, Wideband bow-tie antenna with increased gain and directivity by using a high impedance surface, *Int J RF Microw Comput-Aided Eng* (2019), DOI: 29. e21619. 10.1002/mmce.21619.
 - 9 Wen D, Hao Y, Munoz M, Wang H & Zhou H, A compact and low-profile MIMO antenna using a miniature circular high-impedance surface for wearable applications, *IEEE Trans Antennas Propag*, **66(1)** (2018) 96–104, doi: 10.1109/TAP.2017.2773465.
 - 10 Li L, Wu Z, LiK, Yu S, Wang X, Li T & Li G, Frequency-reconfigurable quasi-sierpinski antenna integrating with dual-band high-impedance surface, *IEEE Trans Antennas Propag* **62(9)** (2014) 4459–4467, DOI: 10.1109/TAP.2014.2331992.
 - 11 Praphat A & Chuwong P, Improved microstrip antenna with HIS elements and FSS superstrate for 2.4 GHz band applications, *Int J Antennas Propag*, **2018**, Article ID 9145373, <https://doi.org/10.1155/2018/9145373>
 - 12 Zhang J, Liu Z, Lu W, Chen H, Wu B, Bian & Liu Q, A low-profile tunable microwave absorber based on graphene sandwich structure and high impedance surface, *Int J RF Microw Comput-Aided Eng*, doi:10.1002/mmce.22022
 - 13 Zhang Y L, Gong H B & Xu Q, The design and simulation of high impedance surface in airborne telemetry antenna, *ITM Web Conf*, **11 08003** (2017) DOI: 10.1051/itmconf/20171108003
 - 14 Praphat A & Chuwong P, Improved microstrip antenna with HIS elements and FSS superstrate for 2.4 GHz band applications, *Int J Antennas Propag* **2018**, Article ID 9145373, <https://doi.org/10.1155/2018/9145373>
 - 15 Zoubiri B, Mayouf A, Devers T & Laouissat M, Improving L-band printed monopole antenna performance using high impedance surfaces, 2019 *6th Int Conf Image Signal Process Appl* (ISPA), 2019, 1–4, doi: 10.1109/ISPA48434.2019.8966826.
 - 16 Fatimah Z & Ali, Analysis of high impedance surface as ground of monopole antenna for bandwidth enhancement, *Proc 3rd Int Conf Electr Electron* (Atlantis Press) 166–171, <https://doi.org/10.2991/eecic-13.2013.39>
 - 17 Goodwill K, Singh N & Kartikeyan M V, Dual-band circular polarized bow tie slotted patch antenna over high impedance surface for wimax application, *Int J Microw Wirel*, (2019) 1–6, <https://doi.org/10.1017/S1759078719001326>
 - 18 Chen N, Shen Y, Dong G & Hu S, Compact scalable modeling of chipless RFID tag based on high-impedance surface, in *IEEE Trans Electron Devices*, **66(1)** (2019) 200–206, doi: 10.1109/TED.2018.2864623.
 - 19 Almutawa A T, Kazemi H & Capolino F, Analyze and design of thin planar high impedance surface as an antenna, *Int Conf Electromagn Adv Appl (ICEAA)* 2018, 623–624, doi: 10.1109/ICEAA.2018.8520480.
 - 20 Sievenpiper D, Zhang L & Yablonovitch E, High-impedance electromagnetic ground planes, 1999 *IEEE MTT-S Int Microw Symp Digest* (Cat. No.99CH36282) **4** (1999) 1529–1532, doi:10.1109/MWSYM.1999.780247.
 - 21 Anand R & Chawla P, A novel dual-wideband inscribed hexagonal fractal slotted microstrip antenna for C- and X-band applications, *Int J RF Microw Comput-Aided Eng*, **30(9)** (2020), doi:10.1002/mmce.22277
 - 22 Vinoy K J, Jose K A, Varadan V K & Varadan V V, Hilbert curve fractal antenna: A small resonant antenna for VHF/UHF applications, *Microw Opt Technol Lett*, **29** (2001) 215–219, <https://doi.org/10.1002/mop.1136>
 - 23 Long J & Sievenpiper D, Dispersion-reduced high impedance surface loaded with non-foster impedances, *IEEE Int Symp Antennas Propag & USNC/URSI Nat Radio Sci Meet* (2015) 69–70, doi: 10.1109/APS.2015.7304420
 - 24 Balanis C, *Antenna Theory*, (Wiley-Interscience, New York) (2005).